BioGecko Vol 12 Issue 03 2023
ISSN NO: 2230-5807

Exact Solution for an Unsteady Flow of Radiative Nanofluid under the Existence of Heat Source in Conducting Field

C. Srinivasulu[1], P. Chandra Reddy[2*], M. Umamaheswar[3], S. Harinath Reddy[4]

[1,2,3,4]Department of Mathematics, Annamacharya Institute of Technology and Sciences, Rajampet, A.P., India – 516126.*

Corresponding Author: P. Chandra Reddy[2]*
Email: chandramsc01@gmail.com

Abstract
An exact solution has been gained for the flow of MHD nano fluid past a vertical porous plate under the impacts of thermal radiation and heat generation with variable temperature. Graphs are used to study and depict the fluctuations in velocity, temperature, and concentration caused by the influence of various physical parameters. Additionally, we have noted the numbers for local skin friction, heat transfer, and mass transfer rates and talked about each one's features. The findings demonstrate that a drop occurs in temperature as the dimensionless solid volume fraction of nanoparticles parameter ∅ is increased.

Keywords: Magnetohydrodynamics; Thermal Radiation; Nanofluid; Porous medium; Heat source.

1. INTRODUCTION

In recent years, many researchers had a great attention towards nanofluids as it has many applications in various fields such as material sciences, medicine, electronics, chemical, civil engineering and so on. This is due to the enhanced thermo physical properties of nanofluids. Nanofluid is characterized as a mixture of base fluid which is suspended with solid nanoparticles of size 1nm to100 nm. It exhibits higher thermal conductivity and convective heat transfer coefficient than the traditional fluids such as water, oil, and ethylene glycol. Physically, the combined effects of heat and mass transfer under the impact of different parameters are mainly utilized in petroleum manufacturing and water purification processes. According to Choi S.U.S. [1], nanofuids are heat transfer fluids that contain nanomaterials (width less than 100 nm) to enhance the qualities of heat transmission. The ultimate goal of nanofluids is to maximise thermal conductivity with the fewest number of nanoparticles possible. Due to a nanofluid's improved thermal conductivity, it was able to cool microchannels without clogging and pump more effectively, among other benefits. Ahmad et al.'s [2] investigation of the nanofluid flow dynamics past a Riga plate used both analytical and numerical methods. They came to the conclusion that the size of the nanoparticles is proportional to the Nusselt number's magnitude. Using a computational method, Sheremet et al. [3] examined how the corner heater affected MHD nanofluid flow in a porous wavy cavity and demonstrated that the magnetic field has a detrimental effect on heat transmission. Chandra Reddy et al. [4,5,6,7] studied and reported MHD nanofluid flow properties past a moving vertical plate in the presence of radiation and thermal diffusion and also MHD natural convective heat generation/absorbing and radiating fluid past a vertical plate

embedded in porous medium. Eid et al. [8,9] gave detailed experimental characterization, TDDFT-DFT, and spin effect on [PEG/H_2O-ZrO_2/TiO_2]^h hybrid nanofluid 3D flow as potential ceramic industry application and also reported on 3D Prandtl nanofluid flow with higher-order chemical reaction.

Mathematical formulation:

An unsteady Nano_Magneto Hydrodynamics fluid radiation free convective heat absorbing/generating fluid with variable temperature has been considered. The x-axis is taken parallel to the channel, while the y-axis is taken perpendicular to it. The B_0uniform magnetic field applied to the flow in a transverse direction. When time $t \leq 0$ the fluid is at rest and the plate is kept at atemperature greater than the surrounding air temperatureT_∞. Temperature drops with temperature $T = \frac{1}{1+at}$ at time $t > 0$ and the plate exponential accelerates with increasing time in its own plane. The species concentration drops with time't' in a similar manner. It is presumpted that the effect of viscous dissipation is minimal and that the boundary layer and standard Boussineq's approximation will work. The flow is controlled by the following equations in light of the aforementioned factors.

$$\rho_{nf}\frac{\partial u^*}{\partial t^*} = \mu_{nf}\frac{\partial^2 u^*}{\partial t^{*2}} + g\rho\beta_{nf}(T^* - T_\infty) - \sigma_{nf}B_0^2 u^* - \frac{\mu_{nf}}{k^*}u^* \quad (1)$$

$$\rho C_{p_{nf}}\frac{\partial T^*}{\partial t^*} = K_{nf}\frac{\partial^2 u^*}{\partial t^{*2}} - \frac{\partial q_r^*}{\partial y^*} + (T^* - T_\infty) \quad (2)$$

The associated initial and boundary conditions of the illustrated model are as follows:

$$\left.\begin{array}{rrrr} t \leq 0: & u^* = 0\,, & T^* = T_\infty\,, & for\ all \quad y^* \leq 0 \\ t > 0: & u^* = U_0 a^* t^*\,, & T^* = T_\infty + \left(\frac{T_S^* - T_\infty}{1+At^*}\right)\,, & at \quad y^* = 0 \\ & u^* = 0\,, & T^* = T_\infty\,, & as \quad y^* \to \infty \end{array}\right\} \quad (3)$$

Where $A = \frac{U_0^2}{\nu}$

Introducing the dimensionless variables and parameters are as follows:

$$\left.\begin{array}{c} U = \frac{u^*}{U_0}\,, y = \frac{y^* U_0}{\nu}\,, t = \frac{t^* U_0}{\nu}\,, \theta = \frac{T^* - T_\infty}{T_S^* - T_\infty}, a = \frac{a^*\nu}{U_0},\ K = \frac{k^* U_0^2}{\nu^2},\ \frac{\partial q_r^*}{\partial y^*} = 4(T^* - T_\infty)I^* \\ M^2 = \frac{B_0^2\sigma_f\nu_f}{\rho_f U_0^2}, G_r = \frac{g\beta_f\nu_f}{U^3}(T_S - T_\infty)\,, F = \frac{4\,I^*\nu_f}{\rho_f C_{p_f} U_0^2}\,, Q = \frac{Q^*\nu_f^2}{K_f U_0^2}, P_r = \frac{\nu_f\,\rho_f\,C_{p_f}}{K_f} \end{array}\right\} \quad (4)$$

We obtain the dimensionless governing system of partial differential equations of the model as follows:

$$a_1\frac{\partial U}{\partial t} = a_2\frac{\partial^2 U}{\partial y^2} - \left(a_3 M^2 + \frac{a_2}{K}\right)U + G_r a_4\theta \quad (5)$$

$$a_5\frac{\partial \theta}{\partial t} = \frac{a_6}{P_r}\frac{\partial^2\theta}{\partial y^2} - \left(F + \frac{Q}{P_r}\right)\theta \quad (6)$$

The analogous initial and boundary conditions becomes:

$$\left.\begin{array}{lll} t \le 0: & U = 0\,,\ \theta = 0\,, & for\ all \quad y \le 0 \\ t > 0: & U = at\,,\ \theta = \frac{1}{1+t}\,, & at \quad y = 0 \\ & U = 0\,, \quad \theta = 0\,, & as \quad y \to \infty \end{array}\right\} \tag{7}$$

Method of solution:

The boundary conditions (7) around the fluid in the plate must be met in order to solve the system of partial differential equations (5) and (6) mentioned above.

$$\left.\begin{array}{l} U = U_0(y) + \varepsilon e^{at} U_1(y) \\ \theta = \theta_0(y) + \varepsilon e^{at} \theta_1(y) \end{array}\right\} \tag{8}$$

Equating the harmonic and non-harmonic terms with (8) in equations (5) and (6), we get

Zeroth order equations:

$$U_0'' - \beta_2 U_0 = -\beta_5 \theta_0 \tag{9}$$

$$\theta_0'' - \beta_4 \theta_0 = 0 \tag{10}$$

First order equations:

$$U_1'' - \beta_3 U_1 = -\beta_6 \theta_1 \tag{11}$$

$$\theta_1'' - \beta_1 \theta_1 = 0 \tag{12}$$

The analogous boundary conditions become:

$$\left.\begin{array}{l} U_0 = at\,,\ U_1 = 0, \quad \theta_0 = \frac{1}{1+t}\,,\ \theta_1 = 0 \quad at \quad y = 0 \\ U_0 \to 0\,,\ U_1 \to 0, \quad \theta_0 \to 0\,,\ \theta_1 \to 0 \quad as \quad y \to \infty \end{array}\right\} \tag{13}$$

Equations (9) through (12) are solved for under initial and boundary conditions (13), and the result is:

$$\theta_0 = L_1 e^{-y\sqrt{\beta_4}} \quad ; \quad \theta_1 = 0 \tag{14}$$

$$U_0 = L_3 e^{-y\sqrt{\beta_2}} + L_2 e^{-y\sqrt{\beta_4}} \quad ; \quad U_1 = 0 \tag{15}$$

Given the aforementioned equations can be expressed as:

$$\theta = L_1 e^{-y\sqrt{\beta_4}} \tag{16}$$

$$U = L_3 e^{-y\sqrt{\beta_2}} + L_2 e^{-y\sqrt{\beta_4}} \tag{17}$$

Skin friction coefficient:

$$\tau = \left(\frac{\partial U}{\partial y}\right)_{y=0} = -\left(\sqrt{\beta_2}\, L_3 + \sqrt{\beta_4}\, L_2\right) \tag{18}$$

Rate of heat transfer coefficient:

$$N_u = \left(\frac{\partial \theta}{\partial y}\right)_{y=0} = -\sqrt{\beta_4}\, L_1 \tag{19}$$

2. RESULTS AND DISCUSSION:

Exact solution by using perturbation method is derived for velocity and temperature under the impacts of a variety of parameters, including $M,\ F, \emptyset, P_r, K,\ a, t$ velocity, temperature skin friction, and nusselt number, and the results are graphically displayed in Figures (1) through (9). The effects of the dimensionless solid volume fraction of nanoparticles parameter $\emptyset$ are shown in Figure 1. This graph demonstrates that velocity decreases as the dimensionless solid volume fraction of nanoparticles parameter.

The impact of the Prandtl number P_r on the velocity distribution is shown in Figure (2). It is observed that the velocity falls off as the Prandtl number $P_r$rises. This is due to the fact that low Prandtl number P_r fluids have high thermal diffusivity, which leads to greater temperatures in constant state. This, in turn, results in stronger buoyancy force, or higher fluid velocity, compared to fluids with relatively low Prandtl numbersP_r. In figure (3), the effect of the magnetic parameter M is depicted visually. The mean velocity drops as the magnetic parameter increases, as expected. The transverse magnetic field's influence produces a drag-like resistive type of force that tends to oppose the viscoelastic fluid's tendency to move more slowly.

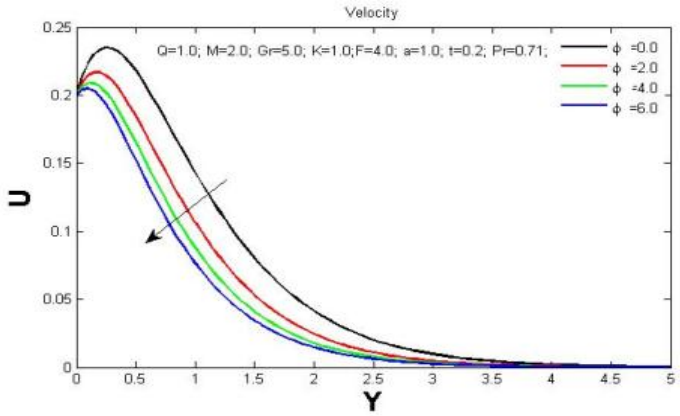

Fig-1: velocity distributions for various values of $\emptyset$

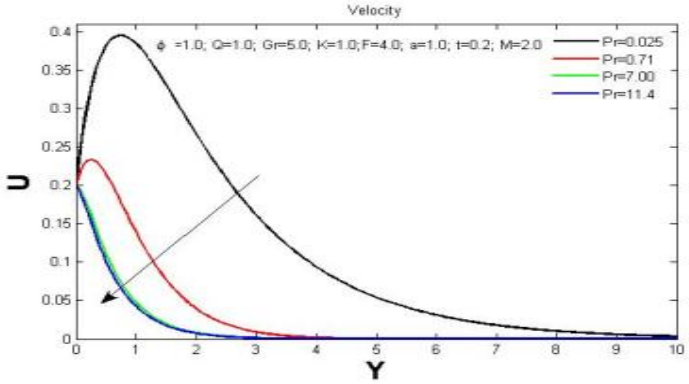

Fig-2: velocity distributions for various values of P_r

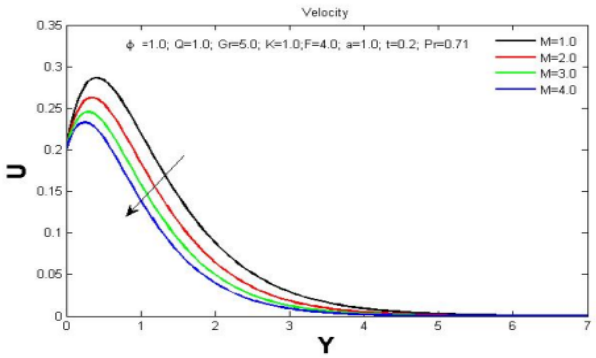

Fig-3: velocity distributions for various values of M

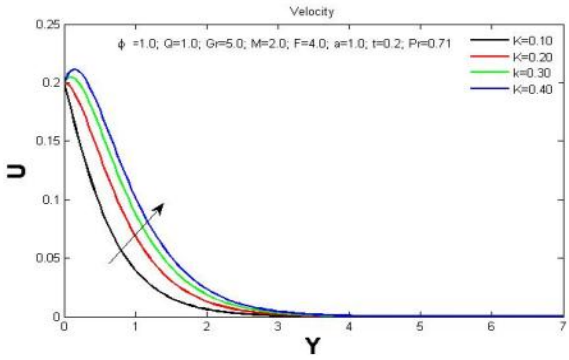

Fig-4: velocity distributions for various values of K

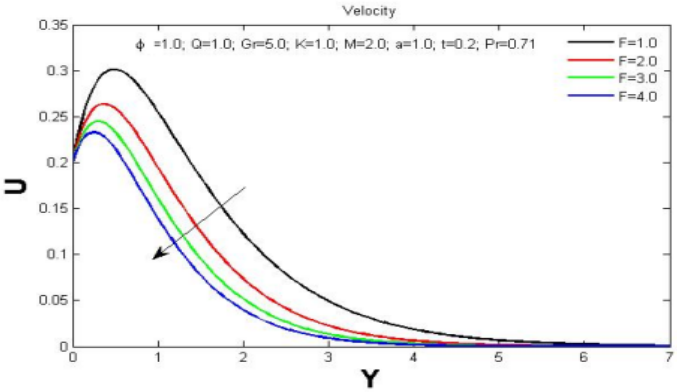

Fig-5: velocity distributions for various values of F

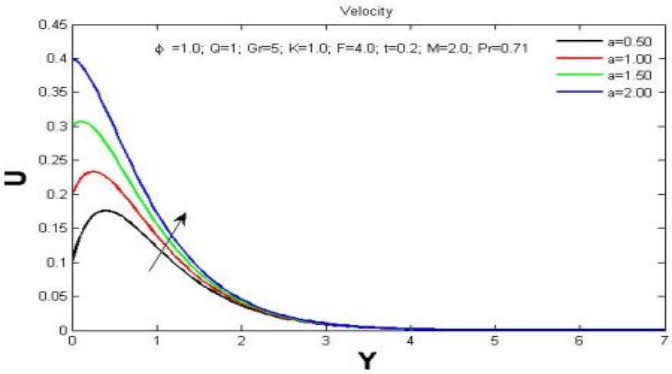

Fig 6: velocity distributions for various values of a

Figure (4) shows the fluctuation of velocity profiles with a dimensionless permeability parameter K. This graph unequivocally shows that as the dimensionless permeability parameter K is raised, the value of velocity profiles diminishes. The impact of the radiation parameter on the velocity distribution is shown in Figure (5). With rising radiation parameter values, it is shown that the velocity decreases. The velocity profiles for various values of the accelerating parameter "a" are shown in Figure (6). The figure shows that the velocity rises as the accelerating parameter rises. Additionally, it is discovered that the fluid velocity caused by an exponentially accelerated start (accelerating parameter not equal to zero) is greater than that caused by an impulsive start of the plate (accelerating parameter equal to zero).

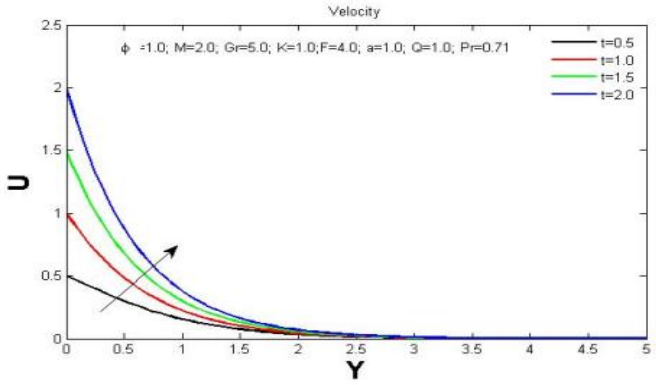

Fig-7: velocity distributions for various values of t

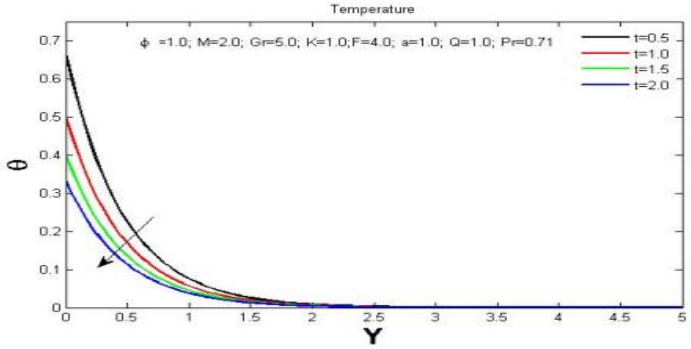

Fig-8: temperature distributions for various values of t

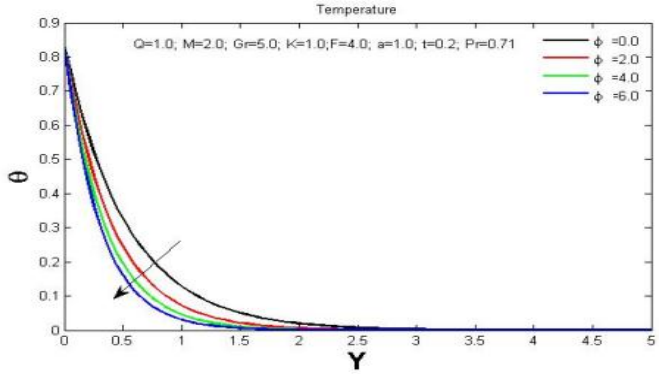

Fig-9: temperature distributions for various values of ∅

The effects of the dimensionless time parameter "t" are seen in Figure (7). This graph shows that as the dimensionless time parameter is increased, velocity continues to climb. Figure (8) illustrates typical temperature profile fluctuation for various values of the dimensionless time parameter t. The findings demonstrate that a drop occurs as the dimensionless time parameter is increased. In the case of heat-absorbing fluids, the momentum and thermal boundary layers consequently get thinner. Figure (9) illustrates typical temperature profile fluctuation for various values of the dimensionless solid volume fraction of nanoparticles parameter ∅. The findings demonstrate that a drop occurs as the dimensionless solid volume fraction of nanoparticles parameter ∅ is increased.

3. REFERENCES

[1]. Choi, S. US, and Jeffrey A. Eastman. Enhancing thermal conductivity of fluids with nanoparticles. No. ANL/MSD/CP-84938; CONF-951135-29. Argonne National Lab.(ANL), Argonne, IL (United States), (1995).

[2]. Ahmad A, Asghar S, Afzal S (2016) Flow of nanofluid past a Riga plate. J Magn Magn Mater 402:44–48.

[3]. Sheremet MA, Oztop HF, Pop I (2016) MHD natural convection in an inclined wavy cavity with corner heater filled with a nanofluid. J Magn Magn Mater 416:37–47.

[4]. Chandra Reddy P, Raju MC, Raju GSS. MHD Natural convective heat generation/absorbing and radiating fluid past a vertical plate embedded in porous medium - an exact solution. *Journal of the Serbian Society for Computational Mechanics*. 2018;12(2):106–127.

[5]. Chandra Reddy P, Raju MC, Raju, Varma, Raju GSS. Free convective magneto-nanofluid flow past a moving vertical plate in the presence of radiation and thermal diffusion. *Frontiers in Heat and Mass Transfer, Int. Journal*. 2016;7(28):1-7.

[6]. Chandra Reddy P, Umamaheswar M, Harinath Reddy S, Raju MC. Analytical study of buoyancy effects on MHD visco-elastic fluid past an inclined plate. *AIP Conference Proceedings*. 2020;2246(020072):1-7; https://doi.org/10.1063/5.0014572.

[7]. Chandra Reddy P, Venkateswara Raju K, Umamaheswar M, Raju MC. Buoyancy effects on chemically reactive magneto-nanofluid past a moving vertical plate. *Bulletin of Pure and Applied Sciences*. 2019;38(1):193-207.

[8]. Eid MR, Ali MA, Al-Hossainy AF. Experimental characterization, TDDFT-DFT, and spin effect on $[PEG/H_2O\text{-}ZrO_2/TiO_2]^h$ hybrid nanofluid 3D flow as potential ceramic industry application. *International Journal of Chemical Reactor Engineering*. 2021;19(11):1135-1149. https://doi.org/10.1515/ijcre-2021-0124.

[9]. Eid MR, Mabood F, Mahny KL. On 3D Prandtl nanofluid flow with higher-order chemical reaction. *Journal of Mechanical Engineering Science*.2021;235(19):3962-3974. https://doi.org/10.1177/2F0954406220975429.